AGU PUBLICATIONS

Geophysical Research Letters

RESEARCH LETTER
10.1002/2014GL059532

Key Points:
- Provide confidence and rationale in the robust changes of precip extremes
- Show sign of convergence for certain categories of precipitation extremes

Supporting Information:
- Readme
- Readme2
- Table S1
- Figure S1
- Figure S2

Correspondence to:
J. Lu,
Jian.Lu@pnnl.gov

Citation:
Lu, J., L. Ruby Leung, Q. Yang, G. Chen, W. D. Collins, F. Li, Z. Jason Hou, and X. Feng (2014), The robust dynamical contribution to precipitation extremes in idealized warming simulations across model resolutions, *Geophys. Res. Lett.*, *41*, 2971–2978, doi:10.1002/2014GL059532.

Received 14 FEB 2014
Accepted 2 APR 2014
Accepted article online 3 APR 2014
Published online 17 APR 2014

The robust dynamical contribution to precipitation extremes in idealized warming simulations across model resolutions

Jian Lu[1], L. Ruby Leung[1], Qing Yang[1], Gang Chen[2], William D. Collins[3], Fuyu Li[3], Z. Jason Hou[1], and Xuelei Feng[4]

[1]Pacific Northwest National Laboratory, Richland, Washington, USA, [2]Department of Earth and Atmospheric Sciences, Cornell University, Ithaca, New York, USA, [3]Lawrence Berkeley National Laboratory, Berkeley, California, USA, [4]Department of Atmospheric, Oceanic, and Earth Sciences, George Mason University, Fairfax, Virginia, USA

Abstract The impact of the circulation shift under climate warming on the distribution of precipitation extremes and the associated sensitivity to model resolution are investigated using Community Atmosphere Model Version 3.0 in an aquaplanet configuration. The response of the probability density function of the precipitation to a uniform sea surface temperature warming can be interpreted as superimposition of a dynamically induced poleward shift and a thermodynamically induced upward shift toward higher intensities, which give rise to manyfold increase in the frequency of the most extreme categories of the precipitation events at the poleward side of the midlatitude storm track. Coarser resolutions underestimate not only the intensity of the precipitation extremes but also the dynamical contribution to the increase of precipitation extremes. Meanwhile, the thermodynamic contribution to the intensification of the precipitation extremes is substantially less than expected from the Clausius-Clapeyron relation, implicative of significant change in the vertical structure of the precipitation processes.

1. Introduction

Precipitation extremes have been a topic of intensive studies because of their disproportionally large socioeconomic impacts. While the intensification of precipitation extremes under climate warming has been mostly attributed to the increased water vapor-holding capacity [e.g., *Trenberth et al*., 2003; *Emori and Brown*, 2005; *Kharin et al*., 2013], how atmospheric dynamical changes may have an imprint on precipitation extremes remains unclear. Given that the meridional expansion and/or shift of the key large-scale features of the global circulation are the most robust aspects of the climate change response [e.g., *Lu et al*., 2007; *Lorenz and DeWeaver*, 2007a], the circulation change will inevitably impact the statistics of the subtropical and midlatitude extremes. The latest estimation of the 50 year return level of precipitation extreme from the simulations of the Coupled Model Intercomparison Project Phase 5 (CMIP5) models suggested an up to 50% increase in the middle to high latitudes [*Toreti et al*., 2013]. But no physical/dynamical rationale was provided for this super Clausius-Clapeyron rate of increase. *Kang et al*. [2013] investigated the impacts of stratospheric ozone depletion on precipitation extremes in austral summer and found that ozone-induced changes in precipitation extremes are predominantly dynamical rather than thermodynamical in origin. In view of the fact that the circulation response to global warming in the extratropics shares similar spatial structure as that to ozone depletion in the Southern Hemisphere (SH), we set out to investigate the dynamical contribution to the change of the distribution of precipitation extremes under global warming-like SST warming in an idealized modeling framework.

Climate model simulations of extreme precipitation are sensitive to physics parameterizations for subgrid processes such as convection and clouds, representation of the cross-scale energy and enstrophy cascades, and model resolution. As the typical resolution of the current generation of climate models are far from convergence on these physical and dynamical processes important for precipitation extremes, the ability of the climate models in capturing the full probability density function (PDF) of precipitation events is still an open question [*Randall et al*., 2007]. *Li et al*. [2011a, 2011b] demonstrated a promising sign of resolution convergence in the midlatitude precipitation extremes under simple SST warming perturbations in an aquaplanet atmospheric general circulation model (AGCM). This study is an extension of *Li et al*. [2011a] on analysis of precipitation extremes in a suite of aquaplanet AGCM simulations with various horizontal

resolutions. New insights are gained by focusing on the meridional structure of the PDF of extremes and quantifying the circulation contribution to the change of the PDF of precipitation.

2. Model Data Sets

The same model data output as *Li et al.* [2011a, 2011b] from a set of idealized aquaplanet simulations with the NCAR Community Atmospheric Model Version 3.0 (CAM3) [*Collins et al.*, 2004] is used in this study. To assess the sensitivity to model resolution, four horizontal resolutions corresponding to spectral truncations of T42, T85, T170, and T340 (~2.8, 1.4, 0.7, and 0.35° resolution in the transformed grids, respectively) are used for a triad of experiments: control, 3 K uniform warming (denoted as sstmag), and SST warming with a meridional gradient (denoted as sstgra). In the control run, a zonally symmetric SST profile is prescribed following *Neale and Hoskins* [2000].

$$\mathrm{SST}(\varphi) = \begin{cases} 27\left(1 - \sin^2\left(\frac{90}{60}\varphi\right)\right) & \text{if } |\varphi| < 60°, \\ 0 & \text{if } |\varphi| > 60°. \end{cases} \quad (1)$$

In experiment "sstmag," the SST profile (1) is perturbed by a uniform 3 K increase. The SST forcing for experiment "sstgra" is prescribed as

$$\mathrm{SST}(\phi) = \begin{cases} 30\left(1 - \sin^2\left(\frac{90}{60}\varphi\right)\right) & \text{if } |\varphi| < 60°, \\ 0 & \text{if } |\varphi| > 60°. \end{cases} \quad (2)$$

The simplicity in the SST perturbations will facilitate the scaling analysis and the interpretation thereof in the following section. Note that the direct effect of increase in greenhouse gases is not considered in these sets of simulations.

The simulations periods are 8, 4, 2, and 2 years for all the control and perturbation runs at each of the four grid resolutions. The inverse relationship between spatial resolution and simulation period (with the exception of T340) is to take advantage of the zonal symmetry in the aquaplanet world as the number of grid points in the zonal direction doubles with each refinement of resolution. Because the insolation and the radiatively active species are held fixed in an equinoctial and hemispherically symmetric geometry, the statistics of the model climate are zonally and hemispherically symmetric. In the PDF-based analysis below, the SH data are reflected to the Northern Hemisphere so as to double the sample size and the result is shown hemispherically. However, for the percentile-based analysis, results are presented for both hemispheres and the agreement between the two hemispheres gives a sense of sampling adequacy. (Due to the internal mode of variability, simulation over a small number of years is not sufficient to smooth out the noise associated with these dynamical modes and the statistics based on a limited time period between the two hemispheres may differ). Daily precipitation, 500 hPa omega (ω_{500}), and column-integrated precipitable water are among the variables outputted and hence are used for the current analysis.

3. Analysis and Results

3.1. PDF Approach

We first estimate the PDF of precipitation by computing the histogram using equally spaced bins (1 mm d^{-1}) spanning from 0 through 240 mm d^{-1}. The resulting PDFs of the control simulations are displayed in $\log_{10}$ scale as contours in Figure 1 for all four resolutions. To focus on the midlatitudes, only bins less than 120 mm d^{-1} are shown. The 10^{-4} frequency events, which correspond to extreme values with return period of 10,000 days, are tenably sampled at all four resolutions given the sample size of 368,640 for each latitude for the T42, T85, and T170 simulations, and 737,280 for the T340 simulation. Comparing across resolutions, one can see obvious deficiency of the T42 resolution in simulating the intensity of the 10^{-4} frequency events, but the other three resolutions appear to converge on the intensity of the 10^{-3} frequency or even 10^{-4} frequency events in the extratropics. Overall, the more the extremes are, the greater the challenge is for the coarser resolution model to capture their values. The shadings in Figure 1 show the $\log_{10}$ of the PDFs of the sstmag simulations normalized by the corresponding control PDF, indicating the effect of 3 K SST warming on the

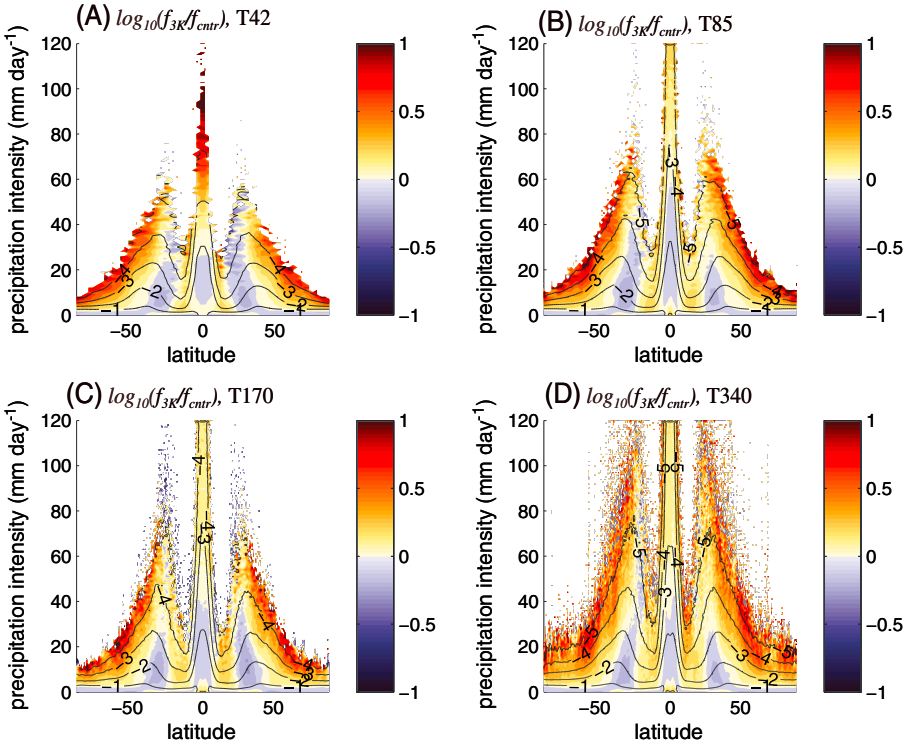

Figure 1. Change of the probability density function of daily precipitation in response to 3 K SST warming simulated by CAM3 at (a) T42, (b) T85, (c) T170, and (d) T340 resolution. The change (shaded) is expressed as the logarithm of the PDF normalized by the control PDF. In each panel, the corresponding control $\log_{10}$(PDF) is overlaid as black contours.

precipitation PDF. Despite the deficiency of the coarser resolutions in capturing the intensities of the rarest events, all four resolutions show similar characteristics of (i) reduction in the frequency of the modest extremes at the equatorward flank of the mean storm track and (ii) increase in the frequency of all extremes at the poleward flank of the storm track and (iii) less frequent weak precipitation events at the middle to high latitudes. It is interesting to note that all these three features of the precipitation PDF change are also shared by the change of the PDFs of ω_{500} (see Figure S1a in the supporting information).

The propensity of the meridional shift is even clearer in the PDF of ω_{500} (Figure S1a). By minimizing the variance of the residual of the fractional change of ω_{500} from fitting the total PDF change to the PDF anomaly that results from a meridional shift of the PDF, i.e., $\left\{\sum_i\left[\frac{\delta f(\omega_i)-\delta f^{\text{fit}}(\omega_i)}{f(\omega_i)}\times\omega_i\right]^2\right\}$, where δf is the total change of PDF (Figure S1a), $\delta f^{\text{fit}} \equiv f(y-\delta y)-f(y)$, denoting the fitted change of PDF that results from a meridional shift by δy (Figure S1b), and ω_i is the value of ω_{500} at bin i, we yield an optimal shift of the PDF of 2.7° in latitude, which, not coincidentally, is the same amount of the shift of the zonal mean zonal wind simulated under the 3 K warming. The similar agreement between the shift of the PDF of ω_{500} and that of the zonal wind is also found in the T42, T85, and T170 simulations, suggesting strongly that the shifts in the zonal mean zonal wind and the transients are integral parts of one circulation change (see Table S1). Provided that the poleward shift in the precipitation distribution can be ascribed to the shift of the circulation and that the thermodynamic effect only manifests in the intensification of the precipitation through the increase of water vapor, one can express the change of the precipitation PDF, a function of the precipitation intensity p and meridional distance y, as

$$\delta f(p,y) = \left[f\left(\frac{p}{1+\varepsilon},y\right)-f(p,y)\right]-\frac{\partial f(p,y)}{\partial y}\delta y+\text{res}, \tag{3}$$

where the terms in the bracket represent the difference resulted from the thermodynamically induced stretching toward more intense precipitation bins and the second term the dynamically induced poleward shift of the PDF (with the change of the intensity of circulation ignored). The stretching factor $\epsilon = \frac{\delta p}{p}$, which

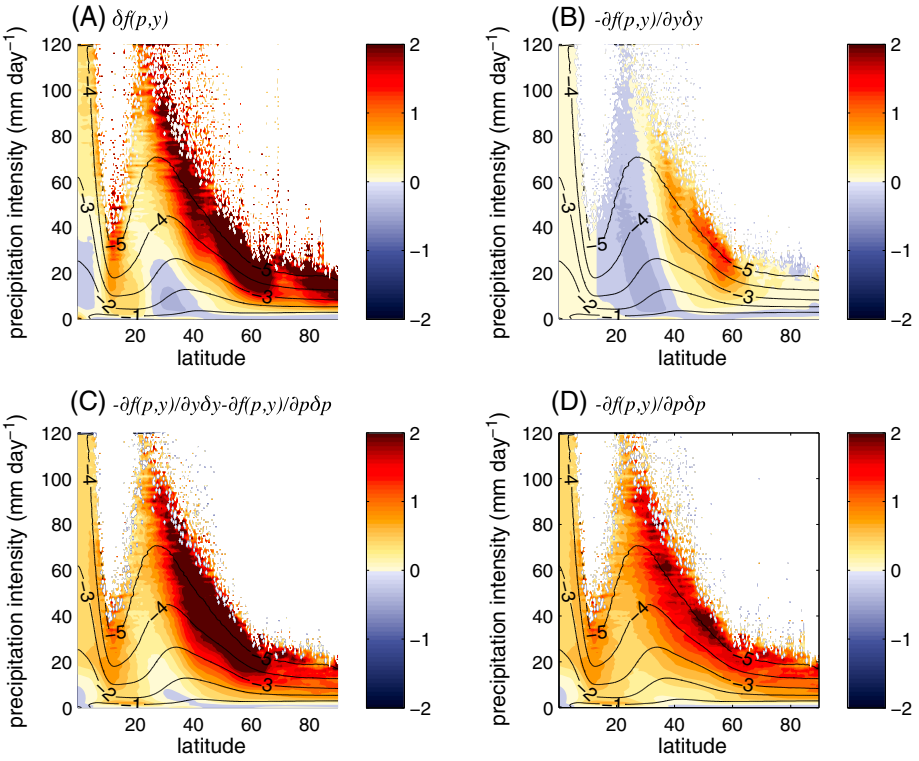

Figure 2. Fractional change of the probability density function of daily precipitation in response to 3 K SST warming in T340 CAM3 simulations. In each panel, the control $\log_{10}$ (PDF) is overlaid as black contours. The color contours are for (a) total change, (b) change due to a poleward shift of the 500 hPa ω PDF, (c) the sum of the changes in Figures 2b and 2d, and (d) change due to the increase of moisture inferred from the depreciated CC rate. Both Figures 2b and 2d are derived from minimizing the error of fitting equation (3) to the simulated PDF changes.

indicates the fractional increase of precipitation intensity, were it following the Clausius-Clapeyron (CC) relation, would be scaled as

$$\epsilon \approx LR_v^{-1}T_0^{-2}\delta T, \tag{4}$$

where L is the latent heat of vaporization, R_v is gas constant for water vapor, δT is 3 K for the sstmag experiments, and T_0 is chosen to be the local SST. The corresponding CC slope, $\alpha = \frac{\delta p}{p}/\delta T$, ranges approximately 7 to 8% per Kelvin warming for the control SST profile (1). The actual stretching factor, however, is estimated together with the shift factor δy by minimizing the fractional variance associated with the residual term in (3) and turns out to be markedly smaller than the CC rate. Interestingly, the resultant shift δy turns out to be the same as the shift of zonal mean zonal wind as well as the shift of the PDF of ω_{500}.

Figure 2 shows the result of fitting (3) to the change of the precipitation PDF in response to the sstmag forcing at T340 resolution. The fitted PDF change accounts for 90% of the variance of the total fractional precipitation change associated with $\delta f(p, y)$ poleward of 13° latitude, with 45% contributed from the poleward shift. Thus, the poleward shift of the subtropical and midlatitude circulation, together with the attendant shift of the transients, account substantially for the increase (decrease) of precipitation at all intensities at the poleward (equatorward) flank of the mean jet/storm track. It should be noted that the thermodynamic pattern (Figure 2d) and the pattern associated with the poleward shift are not orthogonal to each other and that the former accounts for 80% of total fractional precipitation change variance, with approximately 25% shared between them. At the poleward flank of the mean jet, the dynamical shift and the thermodynamics work in concert to give rise to three times as frequent the 10^{-4} extreme events under 3 K warming as the control. The best fit for the thermodynamics corresponds to $\alpha \approx 5\%$/K or a depreciation of the CC rate by 30%. This depreciation rate is consistent with the earlier scaling analysis on the extremes simulated by the GFDL AM2.1 [*Chen et al.*, 2011] and CMIP3 models [e.g., *O'Gorman and Schneider*, 2009b]. In the latter, the sub-CC rate of the thermodynamic contribution was attributed to the notion that the extreme precipitation scales

with the dependence of the moist-adiabatic derivative of saturation specific humidity ($dq_s/dp|_{\theta^*}$), rather than the water vapor content itself, on temperature. Unfortunately, the lack of vertical resolution of the data sets used here does not allow us to further verify the notion of *O'Gorman and Schneider* [2009b]. This sub-CC thermodynamic contribution is robust for all other simulations at coarser resolutions.

It is also interesting to note that there remains a sizable residual of the precipitation PDF (by subtracting Figure 2c from Figure 2a) that cannot be explained by the fitting (3). Further inspection indicates that this PDF residual (not shown) bears a considerable resemblance to the PDF residual of ω_{500} after fitting for a poleward shift (Figure S1c). The intensification of the vertical motion from 60° and poleward appears to be energized by the local increase of temperature and moisture, and the mechanisms for the intensification of the precipitation extremes there seem to be distinct from those of the lower latitudes. In addition, there is discernible weakening in the residual PDFs, reflecting an overall weakening of the transient activity in the midlatitude storm track besides the poleward shift. These two features of circulation change are not considered in the PDF fitting approach above. Next, in the percentile approach, we will take full account of the change of circulation in the scaling for the precipitation percentiles.

3.2. Scaling Precipitation Percentiles

An alternative approach to evaluate the precipitation extremes is to compute the mean values of the scaling factors conditioned on extreme precipitation occurring [e.g., *O'Gorman and Schneider*, 2009a, 2009b]. According to the two-layer model of the atmosphere wherein the moisture is confined in the lower layer and the accumulated precipitation during a given extreme event is determined by the low-level convergence of moisture [*Stevens and Lindzen*, 1978; *Wilson and Toumi*, 2005], the intensity of precipitation extremes can be expressed as

$$p^e = \gamma^e (w^e q^e)_{z_m}, \tag{5}$$

where γ is the precipitation efficiency, representing the fraction of the vertical moisture flux at the top of the moist layer (z_m) that is precipitated out, the superscript e indicates the conditional mean on certain percentile of the precipitation extremes (to be elaborated below following equation (6)). Since the specific humidity data are unavailable at the top of the moist layer, for the actual scaling analysis we use column-integrated precipitable water for q^e. The resulting scaling formula for the fraction change of precipitation extremes turns out to be the same as that used in *Sugiyama et al*. [2010]:

$$\frac{\delta p^e}{p^e} = \frac{\delta \omega^e}{\omega^e} + \frac{\delta q^e}{q^e} + \frac{\delta \gamma^e}{\gamma^e}, \tag{6}$$

where midtropospheric pressure velocity (ω) is used and the *precipitation efficiency* γ^e assumes a similar physical meaning to the parameter a in (1) of *Sugiyama et al*. [2010], which represents the moisture convergence normalized by the column precipitable water and midlevel vertical velocity, thus containing the knowledge of the vertical structures of the moisture and vertical velocity. For brevity, however, we still refer to γ^e as precipitation efficiency. In evaluating the scaling parameters in (6) except the last term, which is deduced as a residual, the conditional mean for a given precipitation percentile is taken over all days and longitudes for which the precipitation lies in a finite range, chosen for the nth percentile as the range between the $100 - \frac{3}{2}(100 - n)$ and $100 - \frac{1}{2}(100 - n)$ percentiles [*O'Gorman and Schneider*, 2009b].

The changes of the 99th and the 99.9th percentiles of precipitation in response to 3 K warming and their respective decomposition into the circulation, column water vapor and precipitation efficiency are presented in Figures 3a and 3b. Consistent with earlier work, the rate of increase of the precipitation extremes is slower than the increase of moisture, the latter appearing to set the upper limit of the former. Consistent with the PDF approach, the scaling for the percentiles also demonstrates unambiguously the importance of the circulation change in shaping the meridional structure of the change of the precipitation extremes. The circulation component is dipolar in character in the subtropical to middle latitudes, with the nodal point shifting progressively equatorward as the percentile increases. As the percentile increases to 99.9th, the thermodynamic component neutralizes the negative dynamical effect at the subtropics resulted from the expansion of the descending branch of the Hadley cell, leading to negligible net change in the intensity of the precipitation extreme there (Figure 3b). The rate of the increase of moisture is overall greater than the CC rate, owing likely to the fact that the troposphere warms more than the surface [*Sugiyama et al*., 2010]. The deviation of the moisture change from the monotonic profile one might expect from the CC scaling (based

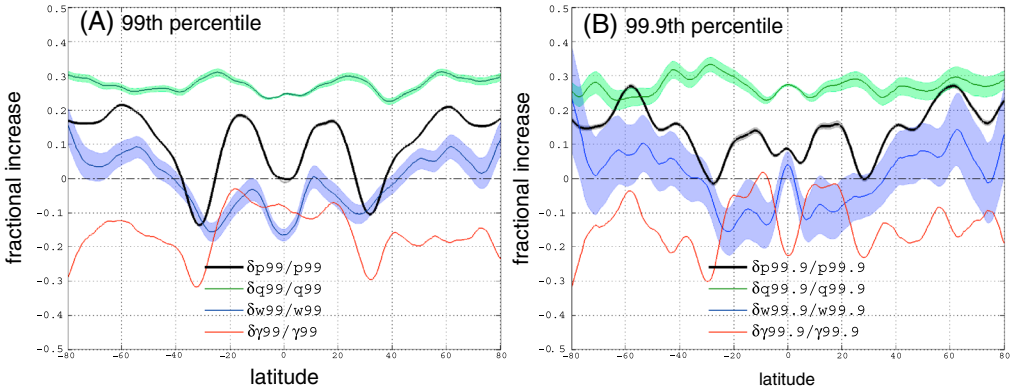

Figure 3. Fractional change of the daily precipitation percentiles (black) and its decomposition into the change of ω_{500} (blue), q (green), and γ^e (red) in response to 3 K SST warming simulated at T340 resolution. (a) The 99th percentile. (b) The 99.9th percentile. Shadings indicate the 99% confidence intervals estimated based on two-tailed Welch's t test.

on the uniform SST warming) can only be attributable to dynamics. A similar dynamical impact on the meridional distribution of column moisture was also evident in the analysis of the mean precipitation and moisture content in *Lorenz and DeWeaver* [2007b, Figure 1]. The dynamical dominance on the spatial structure of the precipitation extremes has important implications for the response of the regional extremes under climate change forcings [e.g., *Kang et al.*, 2013]. Particularly intriguing is the inferred reduction of precipitation efficiency in the middle to high latitudes across a wide range of extremes. Following the interpretation of *Sugiyama et al.* [2010], this might be thought of as the result of the upward transformation of the profile of the circulation that becomes out of sync with the vertical profile of the moisture. The specific aspects related to the vertical profiles warrant future investigation.

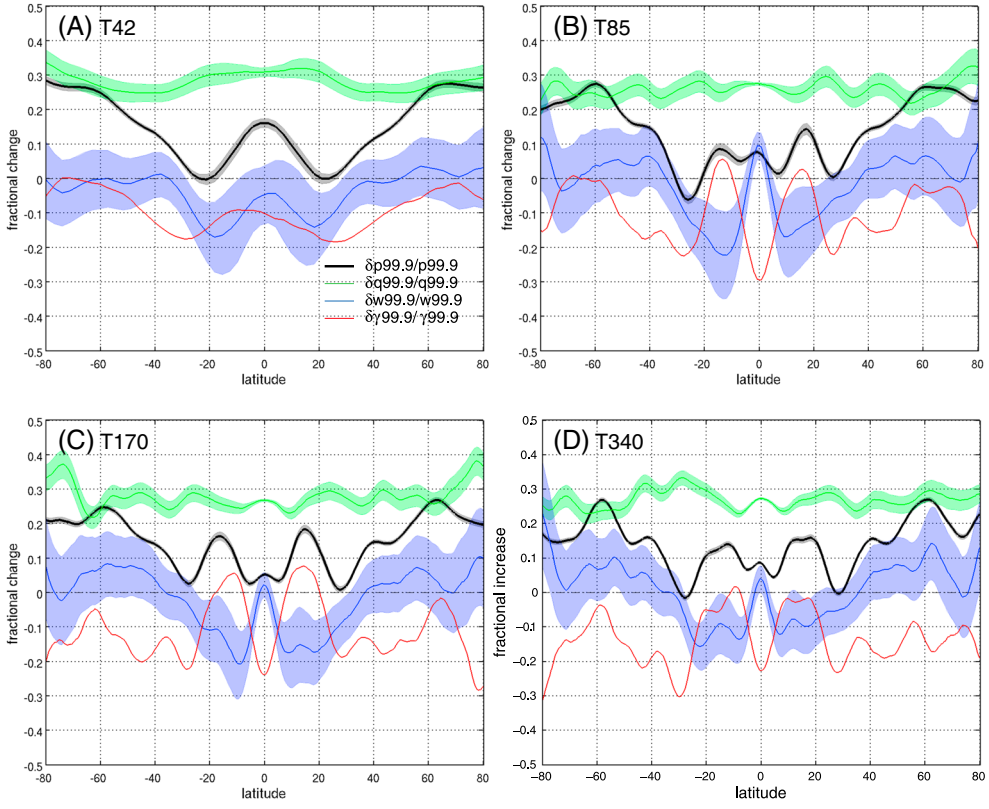

Figure 4. Same as Figure 3b except for (a) T42, (b) T85, (c) T170, and (d) T340 resolutions. Note that Figure 4d is a duplicate of Figure 3b.

The sensitivity of the scaling for the 99.9th precipitation percentile to resolution is examined in Figure 4. The change of the column water vapor shows the least sensitivity to the resolution. T42 has a tendency of underestimating the importance of the dynamical contribution to the precipitation extreme in the midlatitudes while all other higher resolutions show a qualitatively similar dipolar structure in this respect. In fact, the interhemispheric difference within a same resolution is comparable to the interresolution differences among T85, T170, and T340 resolutions. Despite the large sample size, the discernible interhemispheric difference suggests that the simulations are still not long enough for the convergence of the statistics of the 99.9th percentile extreme.

Applying the same percentile analysis to the sstgra experiments shows an even more prominent role of the dynamical shift. If we interpret the contribution from the fractional change of ω as the dynamical contribution and all the remaining as thermodynamical, the former dominates the latter in the precipitation PDF response over the latitudinal range under the influence of the poleward shift of the circulation. As such, a modest increase of the equator-to-pole SST gradient can significantly increase the relative importance of the dynamical contribution to the change of precipitation extremes.

4. Summary and Discussion

Two separate approaches, PDF-based and percentile-based, were applied to analyze the response of the precipitation extremes in a set of aquaplanet simulations under idealized SST boundary forcings at different horizontal resolutions. Both approaches point consistently to a notion that the dynamical shift in circulation contributes substantially to the response of precipitation extremes (in terms of both intensity and frequency) under pseudo climate warming forcing, whereas the thermodynamic contribution is below what the CC relation would suggest, in agreement with the results of *O'Gorman and Schneider* [2009b] and *Chen et al.* [2011]. In the form of the *Wilson and Toumi* [2005], this sub-CC rate of thermodynamics is manifested as reduction of the precipitation efficiency, for which the exact reason belongs to a topic of future investigation. The dynamically induced poleward shift of PDF, in conjunction with the relatively uniform thermodynamical stretch (in the intensity dimension), can give rise to manyfold increase in the frequency of the most extreme categories of the precipitation events at the poleward side of the midlatitude storm track. In addition, this conclusion appears to be independent of the horizontal resolution of the model once the resolution is as fine as T85 and beyond. This might serve as a possible rationale for the factor of 2–3 of reduction in the return period of the 20 year return value of daily precipitation in and poleward of the midlatitude storm tracks reported in the Fifth Assessment Report of the Intergovernmental Panel on Climate Change (see Figure 12.27, Chapter 12).

Superficially, these results appear to be contradictory to the earlier studies that attributed the increase of the extratropical precipitation extremes mostly to thermodynamic causes [e.g., *Gastineau and Soden*, 2009; *Emori and Brown*, 2005]. To reconcile with the earlier works, we note that *Gastineau and Soden* [2009] did not look into the meridional structure but treated the extremes in the extratropics between 30° and 90° as a whole. In addition, we note that as a larger equator-to-pole SST gradient brings about a greater dynamical contribution to the increase of the precipitation extremes (as epitomized by the sstgra experiments), the real-world global warming with polar amplification is reconcilable with the lesser importance of dynamics found in the earlier studies. It is also worth noting that the exact conclusion of *Emori and Brown* [2005] is dictated by the P-ω relationship at the high tail of ω, which is poorly resolved given the limited sample size. Our attempt of applying their scaling to the precipitation percentiles yielded quite sensitive results to the assumption made about the P-ω relationship at high intensities. Therefore, we argue that the approach of *Emori and Brown* [2005] may not be reliable for quantitative assessment for the response of the precipitation extremes.

Acknowledgments

The data for this study, archived at DOE's NERSC data archive system HPSS, can be made available upon request. Data set names: data_aqua, data_aqua_sst, and data_aqua_sstgra. This study was supported by the Office of Science of the U.S. Department of Energy as part of the Regional and Global Climate Modeling program. The Pacific Northwest National Laboratory is operated for DOE by Battelle Memorial Institute under contract DE-AC05-76RL01830. G. Chen is partly supported by the NSF grant ATM-1064079.

The Editor thanks two anonymous reviewers for their assistance in evaluating this paper.

References

Chen G., Y. Ming, N. D. Singer, and J. Lu (2011), Testing the Clausius-Clapeyron constraint on the aerosol-induced changes in mean and extreme precipitation, *Geophys. Res. Lett.*, *38*, L04807, doi:10.1029/2010GL046435.

Collins, W. D., et al. (2004), Description of the NCAR Community Atmosphere Model (CAM3), Tech. Note NCAR-TN-464+STR, Natl. Cent. for Atmos. Res., Boulder, Colo.

Emori, S., and S. J. Brown (2005), Dynamic and thermodynamic changes in mean and extreme precipitation under changed climate, *Geophys. Res. Lett.*, *32*, L17706, doi:10.1029/2005GL023272.

Gastineau, G. and B. J. Soden (2009), Model projected changes of extreme wind events in response to global warming, *Geophys. Res. Lett.*, *36*, L10810, doi:10.1029/2009GL037500.

Kang, S. M., L. M. Polvani, J. C. Fyfe, S.-W. Son, M. Sigmond, and G. J. P. Correa (2013), Modeling evidence that ozone depletion has impacted extreme precipitation in the austral summer, *Geophys. Res. Lett.*, *40*, 4054–4059, doi:10.1002/grl.50769.

Kharin, V. V., F. W. Zwiers, X. Zhang, and M. Wehner (2013), Changes in temperature and precipitation extremes in the CMIP5 ensemble, *Clim. Change*, *119*, 345–357.

Li, F., W. D. Collins, M. F. Wehner, D. L. Williamson, and J. G. Olson (2011a), Response of precipitation extremes to idealized global warming in an aqua-planet climate model: Towards a robust projection across different horizontal resolutions, *Tellus*, *63A*, 876–883.

Li, F., W. D. Collins, M. F. Wehner, D. L. Williamson, and J. G. Olson (2011b), Impact of horizontal resolution on simulation of precipitation extremes in an aqua-planet version of Community Atmospheric Model (CAM3), *Tellus*, *63A*, 884–892.

Lorenz, D. J., and E. T. DeWeaver (2007a), Tropopause height and zonal wind response to global warming in the IPCC scenario integrations, *J. Geophys. Res.*, *112*, D10119, doi:10.1029/2006JD008087.

Lorenz, D. J., and E. T. DeWeaver (2007b), The response of the extratropical hydrological cycle to global warming, *J. Clim.*, *20*, 3470–3484.

Lu, J., G. Vecchi, and T. Reichler (2007), Expansion of the Hadley cell under global warming, *Geophys. Res. Lett.*, *34*, L06805, doi:10.1029/2006GL028443.

Neale, R. B., and B. J. Hoskins (2000), A standard test for AGCMs including their physical parameterizations: I: The proposal, *Atmos. Sci. Lett.*, *1*(2), 101–107, doi:10.1006/asle.2000.0022.

O'Gorman, P. A., and T. Schneider (2009a), Scaling of precipitation extremes over a wide range of climates simulated with an idealized GCM, *J. Clim.*, *22*, 5676–5684.

O'Gorman, P. A., and T. Schneider (2009b), The physical basis for increase in precipitation extremes in simulations of 21st-century climate change, *Proc. Natl. Acad. Sci. U.S.A.*, *106*(35), 14,473–14,477.

Randall, D. A., et al. (2007), Climate models and their evaluation, in *Climate Change 2007: The Physical Science Basis. Contribution of Working Group I to the Fourth Assessment Report of the Intergovernmental Panel on Climate Change*, edited by S. Solomon et al., 996 pp., Cambridge Univ. Press, Cambridge, U. K., and New York.

Stevens, D. E., and R. S. Lindzen (1978), Tropical wave-CISK with a moisture budget and cumulus friction, *J. Atmos. Sci.*, *35*, 940–961.

Sugiyama, M., H. Shiogama, and S. Emori (2010), Precipitation extreme changes exceeding moisture content increases in MIROC and IPCC climate models, *Proc. Natl. Acad. Sci. U.S.A.*, *107*(2), 571–575.

Toreti, A., P. Naveau, M. Zampieri, A. Schindler, E. Scoccimarro, E. Xoplaki, H. A. Dijkstra, S. Gualdi, and J. Luterbacher (2013), Projections of global changes in precipitation extremes from Coupled Model Intercomparison Project Phase 5 models, *Geophys. Res. Lett.*, *40*, 4887–4892, doi:10.1002/grl.50940.

Trenberth, K. E., A. Dai, R. M. Rasmussen, and D. B. Parsons (2003), The changing character of precipitation, *Bull. Am. Meteorol. Soc.*, *84*, 1205–1217.

Wilson, P. S., and R. Toumi (2005), A fundamental probability distribution for heavy rainfall, *Geophys. Res. Lett.*, *32*, L14812, doi:10.1029/2005GL022465.